2008

Short-Range Acoustic Propagation Variability on a Shelf Area with Strong Nonlinear Internal Waves

Reeder, D. Benjamin; Duda, Timothy F.; Ma, Barry

Short-Range Acoustic Propagation Variability on a Shelf Area with Strong Nonlinear Internal Waves

D. Benjamin Reeder
Oceanography Department
Naval Postgraduate School
Monterey, CA 93943 USA

Timothy F. Duda
Applied Ocean Physics and Engineering Department
Woods Hole Oceanographic Institution
Woods Hole, MA 02543 USA

Barry Ma
Department of Marine Science
Naval Academy, Taiwan
P.O. Box 90175, Tsoying District
Kaohsiung, 813 Taiwan

Abstract – **During April 2007 a six-day long experiment was conducted to measure internal waves and their acoustic effects at a continental shelf site in the Northern South China Sea. The site is slightly west of the edge of the shelf. At the shelf edge, large internal waves originating in the Luzon Strait area enter shallow water from deep water, undergoing rapid dissipation and wave shape evolution. A moored acoustic source transmitted 400-Hz pulses 3.0 and 6.0 km to two moored vertical line arrays, with geometry such that the propagation path was roughly parallel to the crests of the strongest passing internal waves, so that strong horizontal refraction effects are expected. Internal-wave characteristics and effects of the internal waves on the sound propagation, both observed and modeled, are shown here.**

I. INTRODUCTION

In spring 2007 a short and focused experiment was performed to investigate acoustic signal variability caused by high-amplitude internal gravity waves near the edge of a continental shelf. The area of study was the northern South China Sea, on the shelf southeast of China. This area has high levels of internal wave activity, with nonlinear waves forming locally from internal tide motions, and with very high energy nonlinear internal waves (also tidally forced) moving up onto the shelf from the direction of the Luzon Strait, which lies directly to the east, Figure 1. The great magnitude of both the westward-propagating internal tides and the nonlinear internal wave packets have been documented in many publications [1-4]. The shape transitions and dissipation of the waves as they encounter the continental shelf are discussed in other papers [5-7].

An important feature of the waves at the experiment site is that they have large amplitudes with respect to the water depth, of the order of one-third the water depth. These large amplitudes are enabled because the internal wave that are incident on the continental slope have amplitudes that exceed the depth of the water on the shelf, and arrive with group velocity faster than the on-shelf group velocity. Much of the wave energy is dissipated because of these factors. However, a large fraction of the remaining wave energy is concentrated in high-amplitude waves with large energy density [7].

The experiment was designed to measure acoustic field fluctuations after only a short propagation distance. Prior experiments have measured strong acoustic fluctuations after a few tens of kilometers of propagation through waters populated with waves of these types [8-12]. After such long propagation distances many intervening bathymetric, internal wave, and frontal features can cause multiple scattering effects. This makes it difficult to verify the effects of individual sound-scattering features. Also short-range experiments are needed to measure effects that occur close to a sound source.

The experiment involved acoustic transmissions between a moored source and two moored receiver arrays. Internal waves were measured with moorings and ship-board instruments. Internal-wave data and sound-field fluctuation data will be shown here, along with results from computational acoustic simulations matched to conditions measured at the site. In this paper, Section II describes the experiment. Section III shows measured internal-wave and sound-field properties. Section IV shows computational acoustic results for observed internal-wave situations. Section V contains a summary.

978-1-4244-2126-8/08/$25.00 ©2008 IEEE

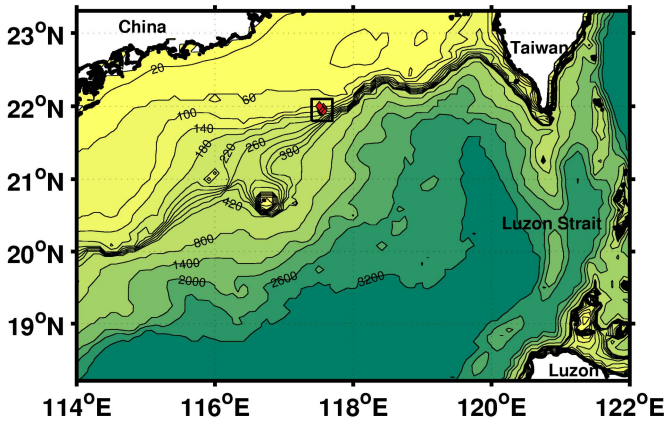

Fig. 1. Chart of the northern South China Sea. The black box indicates our experiment area, which is shown in detail in Figure 2. Strong internal tides and steep tidally-forced nonlinear internal waves cross the deep basin from the Luzon Strait area and encounter the continental slope and shelf a small distance east of the experiment area.

II. Experiment Parameters

The experiment took place between 12 and 22 April, 2007. The Taiwanese research vessel *Ocean Researcher 1 (OR1)*, operated by National Taiwan University (NTU), was used for both the ship-board measurements and to place the moorings. The experiment site lies west of the southern tip of Taiwan (Figure 1). A brief description of the experiment is given here. Further details of the experiment, including depths of instruments and times of observations, are contained in a report [13]. The experiment was linked with other physical oceanographic studies in the area being made by US and Taiwanese scientists, some associated with the US Office of Naval Research NLIWI program.

Eight moorings were placed in a small area east of the edge of continental shelf (Figure 2). The moorings formed a cross, with a vertical line array (VLA) acoustic receiver, V1, at the center. V1 was the central of five moorings on the major line of study at heading 40º, which had an acoustic source at the southwestern end, 3 km from V1 in the center, and another VLA (V2) 3 km from V1 at the northeastern end. S1, V1 and V2 all had vertically spaced thermometers to measure internal waves. Two acoustic Doppler current profilers (ADCPs) were placed near the seafloor between S1 and V1 and between V1 and V2. Arranged close to a line roughly normal to the main mooring line were three moorings measuring temperature only, T1, T2 and T3. Temperature was measured at four depths at S1, V1, V2, T1 and T2, at three depths at T3, and two depths at A1.

The arrangement was chosen so that the direction from S1 to V1 and V2 is roughly parallel with crests of internal waves arriving from Luzon Strait. These arrive at the shelf edge with crests aligned at 10º to 20º, based on satellite images and data from nearby positions [2]. Because of the curved shape of the shelf edge and the slower wave speed on the shelf (~0.65 m/s) compared to deeper water, waves were expected to be rotated at the mooring line to have crests at 25-50º. The S1-V1/V2 path was selected so that sound propagating at an oblique angle to an oncoming internal wave anti-duct (wave of depression, creating a net warm zone with respect to surroundings), with crests at ~35º, might be observed to refract in an anti-clockwise direction and arrive at the VLA momentarily prior to the wave.

The sound source was a 400-Hz Webb Research Corp. projector moored at 102 m depth. This transmitted phase-modulated m-sequence codes, repeating each 5.11 s. From 14 April 0200 UTC (Z) to 15 April 1200 UTC, transmissions lasting 117 s were repeated every 5 minutes. From that ending time until 20 April 0200 UTC, transmissions lasting 13 minutes were repeated every 15 minutes. Both VLA's were manufactured by High Tech, Inc., with Webb Research data recorders. Shipboard observations included acoustic backscatter visualizations of wave shapes with a SIMRAD EK500 38-kHz and 120-kHz instrument, shown in the next section.

III. Wave and Acoustic Field Observations

The arrival times at the experiment site of very large nonlinear internal waves of depression with amplitudes as large as 175 m from the Luzon Strait are now fairly well predictable. Packets of these waves, having only a few members in deep

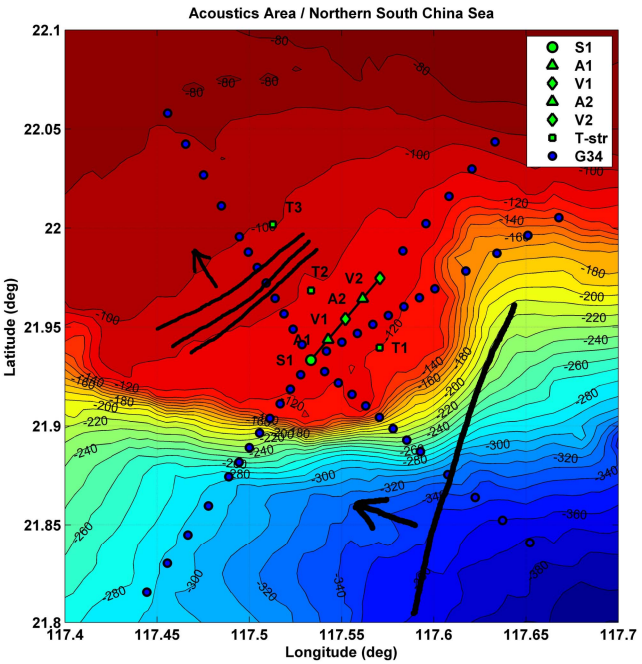

Fig. 2. Chart showing the experiment area. Eight moorings were placed, shown in green. Five are along the acoustic propagation line: S1, acoustic source; A1 (ADCP) 1.48 km from S1; V1 (VLA) 3.00 km from S1; A2 (ADCP) 4.43 km from S1; and V2 (VLA) 6.01 km from S1. The heading along the mooring line is 40° True. Three additional thermometer array moorings were: T1, 2.45 km @ 130° from V1; T2, 2.50 km @ 310° from V1, and T3, 6.66 km @ 322° from V1. The blue dots show intended dipped acoustic source stations. The black lines schematically depict, at the right, an incident internal wave of depression and at the left a packet of waves on the shelf of the type formed from such waves.

978-1-4244-2126-8/08/$25.00 ©2008 IEEE

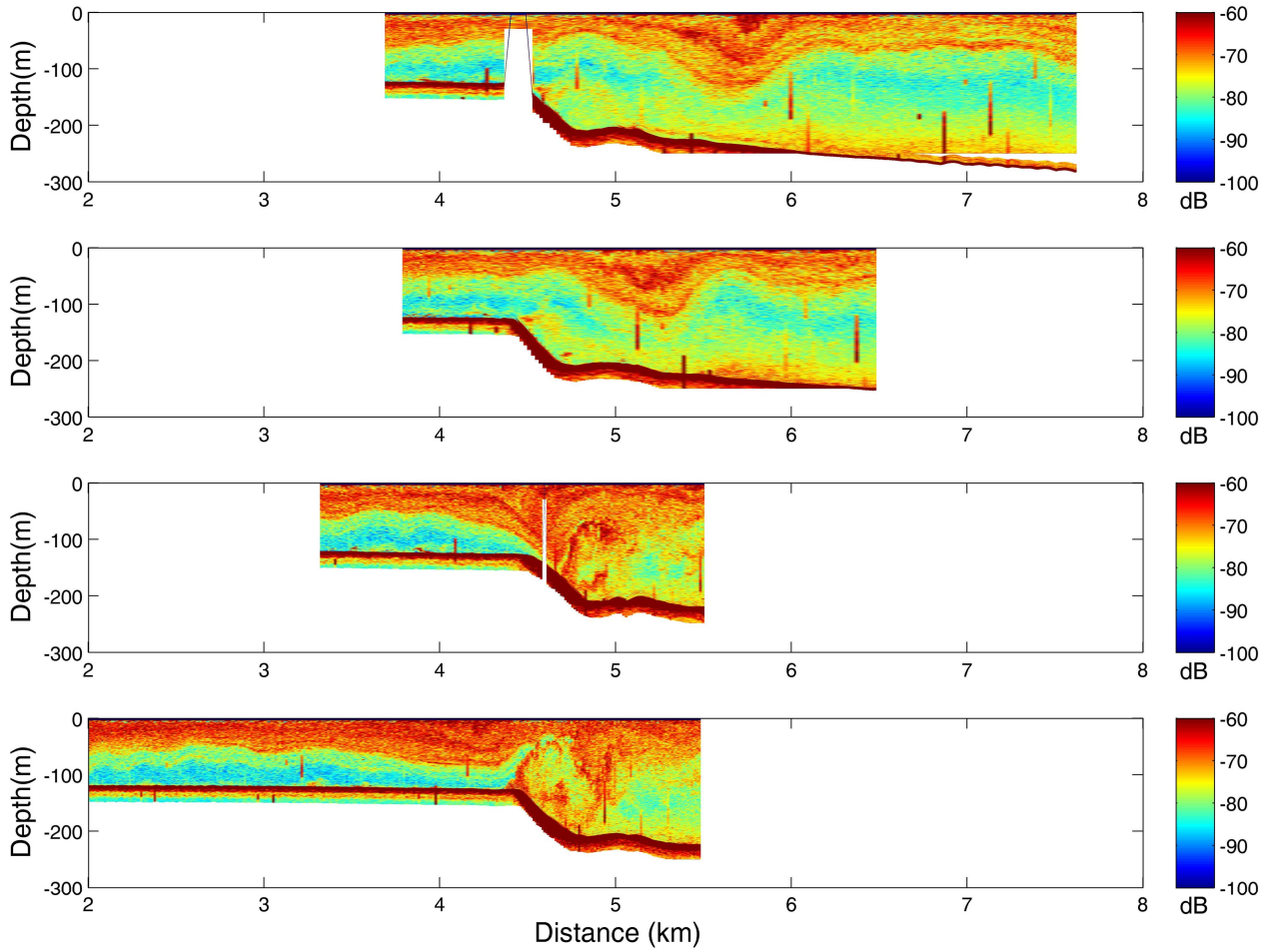

Fig. 3. Acoustic backscatter images collected as *OR1* made repeated transects across one internal wave. The horizontal axis is distance in kilometers, measured along a track at heading slightly north of west, with origin to the east of the data-collection location. Four transects across the wave are shown, with the earliest shown at the top and the latest at the bottom. As the wave approaches the shelf edge near 4.5 km, where the depth at the mooring site (approx 116 m) is attained, the wave becomes asymmetric and loses amplitude. Other observations reveal that a train of steep waves then forms behind the original wave.

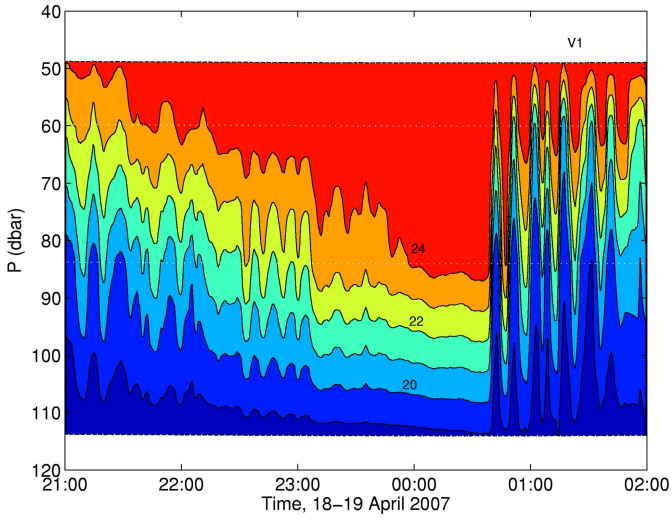

Fig. 4. Contour plot of temperature at V1 for five hours, showing the passing of a large leading internal wave of depression followed by a train of six steep nonlinear internal wave oscillations. Contours from 24º to 19º C are shown.

water, arrive twice per day, after taking a few days to cross the deep water area between the Strait and the experiment site. The experiment was scheduled for a period expected to have strong wave activity after about one day or so of low wave activity.

With the ship positioned to the east of the shelf edge, high-amplitude internal waves were located and followed toward the shelf. The surface roughness caused by interactions of surface waves and internal wave currents, along with acoustic backscatter, allowed the ship to remain with the waves, making repeated transects parallel with the direction of wave propagation. Figure 3 shows backscatter images of a wave first in deep water (at top), and then as it encounters the slope leading up to the shelf. In deep water the wave has amplitude similar to the depth on the shelf, so that the wave profile must transition to a different shape in order for the wave to continue on to the shelf. As with other observations [7,14], and models [15], the single large-amplitude depression wave is seen to become asymmetric, with a gradually sloping front face and a steep back face. Much of the energy of the wave is dissipated. As the depression wave moves onto the shelf, steep nonlinear

978-1-4244-2126-8/08/$25.00 ©2008 IEEE

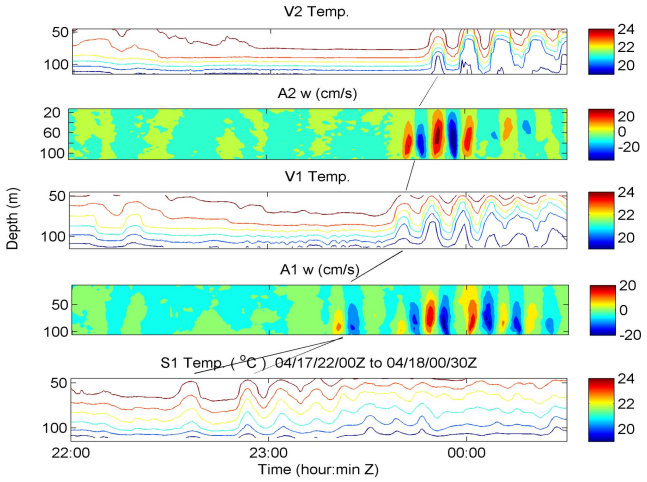

Fig. 5. Measurements of one internal wave packet made along the S1-V2 mooring line are shown. The vertical velocity is shown for A1 and A2. One-degree temperature contours are shown for S1, V1 and V2. The initial wave of elevation following the long wave of depression appears first at S1, as expected, then at A1, V1, A2 and V2. The lines connect the first wave of elevation seen at each station.

waves form behind it, and the broad initial wave of depression broadens but remains intact [5,7,14]. Figure 4 shows the profile of one of these wave groups, the 0000Z 19 April group, at V1. This location is about 6 km onward along the internal wave path from the shelf edge. Figure 5 shows properties of a different wave packet, the 0000Z 18 April group. The figure indicates that that this packet arrived first at S1 and had some curvature, being more parallel to the mooring line at the north end than the south end.

The steep waves following the initial widened depression wave have periods of roughly 10 minutes and amplitudes of about 20 m. These are moving at roughly 0.65 m/s so that they have wavelengths of about 400 m. The trailing-edge waves are evident in satellite images but the broad leading wave is not, leading to the simple viewpoint that the waves converted from depression to elevation, but this is an oversimplification of the actual events.

The short wavelength and high amplitudes of the trailing-edge waves conspire to make them very steep, and capable of producing strong acoustic effects. Sound propagating perpendicular to the crests of waves of this type would exhibit strong coupling of the vertical acoustic normal modes [16]. In this experiment, signals from S1 measured at V1 and V2 would be expected to have undergone refraction of normal modes but no mode coupling [12]. The amount of refraction of each mode depends on the phase velocity gradient (or modal wave number k gradient). The phase velocities vary by 0.33% for mode 1 (critical angle 4.6º) and 0.46% for mode 2 (critical angle 5.5º) for the waves seen near time 01:00 in Figure 4, based on computations with the code KRAKEN. Propagation with strong refraction is expected to result from these strong mode speed gradients. The effect of these ducts is analogous with the ocean sound channel rotated into the horizontal plane from the vertical plane, with many horizontal modes occurring for each vertical mode.

To investigate propagation variability caused by the waves, recordings of the S1 pulses are processed into a reduced form. First, the data are match-filter processed to form complex impulse response time series. The intensity (complex pressure squared) at each phone (each depth z) and of each pulse is then averaged over 0.5 seconds surrounding the peak arrival to form

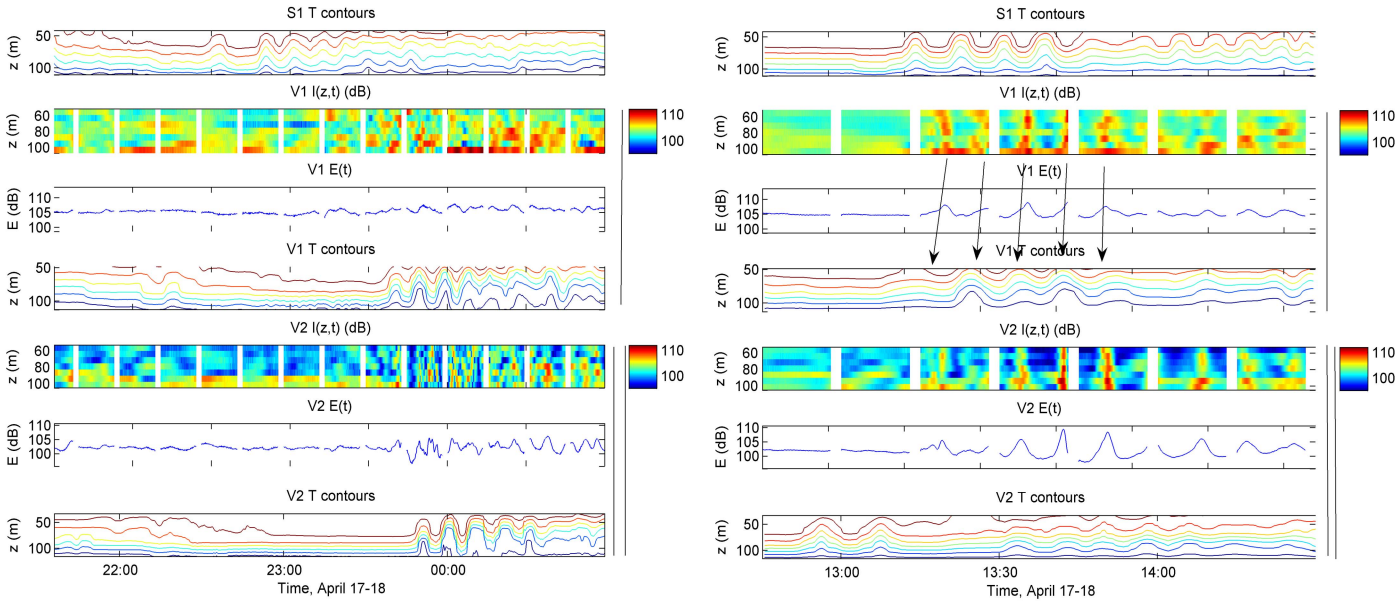

Fig. 6 Acoustic pulse and wave measurements are shown for two time windows. (Left) Window near 0000Z 18 April. (Right) Window of 1230Z to 1530Z 16 April. Shown are: Temperature contours for S1, V1 and V2, depth profiles of intensity $I(z,t)$ for V1 and V2, and depth-integrated intensity $E(t)$.

978-1-4244-2126-8/08/$25.00 ©2008 IEEE

a pulse energy *I(z,t)*. This is then further averaged in depth to form the incoherently depth-averaged energy *E(t)*. Contoured temperature, *I(z,t)* and *E(t)* are shown in Figure 6 for both VI and V2 in two time windows, with S1 temperatures also shown. A packet of large internal waves passes during each time window.

On the right-hand side of Figure 6, the temperatures show that steep waves arrive first at V2, and last at V1, so that there is a bend in the wave. The sound field at V1 goes from a condition with stable bottom-trapped *I,* and stable *E*, to a condition with elevated intensity higher in the water column and fluctuating *E*. Nearly identical signatures of *I* and *E* are seen at V1 and V2, synchronized in time. The periods of high intensity at V1 are seen to correspond to internal waves ducts at the same location, and not with ducts at S1. The ducts occur under wave crests, where cold water is pushed closer to the surface. This is shown by arrows in the plot. This correspondence implies that the sound field leaving the source can enter a duct at low angle within the first few kilometers and then become trapped, with the source not needing to be in the duct. In addition, the focused beams of sound are present at V2 at the same times they are evident at V1, although at V2 the ducts do not appear as strong. The implication of this is that expected strong effects of ducts at ranges of a few kilometers from the source are validated. The net effects of the waves on the energy *E* are losses of a few dB compared to the ambient conditions before the waves, gains of 7 dB or so above the ambient conditions, and oscillations of 10 dB in the waves. Oscillations of *I* in the waves are also of order 10 dB. These results are very similar to those of a prior ~30-160 Hz experiment at 15-km range [12].

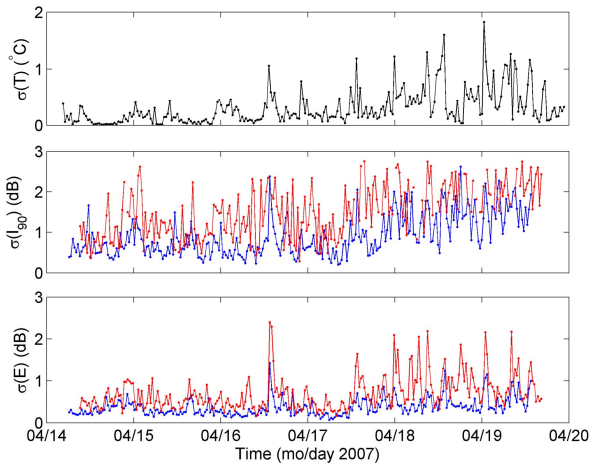

Fig. 7. Acoustic fluctuation statistics are shown for the duration of the experiment. (Lower panel) For time windows approximately ½ hour long, the standard deviation of *E*, which is depth-averaged *I*, is shown in blue for V1 and in red for V2. (Center panel) The standard deviation of pulse intensity *I* at 90 m depth is shown, also with V1 in blue and V2 in red. (Top panel) For the same time windows, the standard deviation of temperature at 83 m depth at V1 is shown as an environmental indicator.

On the left of Figure 6, *I*, *E* and wave profiles are shown for another time window. These are the waves shown in Figure 5. Because of the curvature of the wave packet and its mean misalignment with the S1/V2 line, the source is in the initial wide depression wave in the first part of the interval, while V1 and V2 are in the wave at later times, after 2300. The energy *E* varies much more at V2 than V1. Both sites show strong *I(z,t)* variability. The lower part of the left-hand portion of Figure 6 shows that acoustic variability at V2 corresponds more with the presence of waves at V2 than at S1. From 2300 to 0000, the source is under internal waves, but the V2 arrivals are stable. Note that significant reductions of energy (shadowing) occur at V2 in this set of waves. This is expected because the observed gains at some angles from horizontal focusing require must be balanced by loss at other angles.

Figure 7 shows variance (or standard deviations) of *I* at 90 m depth and *E* in short time windows at both locations. The windows vary in time but average about ½ hour in length (they each contain the same number of measurements). The fluctuations at V2 are stronger than those at V1. Thus, fluctuations build in strength at distances of 3 to 6 km from the source. Note that fluctuations are stronger in the second half of the experiment when internal waves, shown in the lower panel, are stronger. The standard deviation of temperature in 30-min time windows shown in the figure bears similarity with both the *E* and *I* standard deviations computed in similar windows.

IV. Acoustic Field Modeling

Three-dimensional parabolic equation propagation modeling has been carried out using temperature measurements at V1 to construct sound-speed fields typical of the experiment area. The model is described in a report [17]. It implements the wide angle PE [18] with a split-step Fourier solver [19]. The model was run with a 400-Hz source at 102 depth at one end of the Cartesian domain (*x=0*), as in the experiment. Waves traveling in *y*-direction measured at V1 are used to build an *x*-independent sound-speed field (*x* is source-receiver direction). The measurements used are from 17 April 2314:00 to 18 April 0012:30, seen at the left in Figure 6. The experimental domain is about 2 km wide (2048 pts), with computations made to the range of 6000 m (the S1-V2 distance) with steps of one acoustic wavelength. The water depth was 116 m. The same sound speed field and seafloor structure was used for all simulations, with wave movement imitated by changing the source position in the *y* direction. Except for the linear geometry imposed on the internal waves, and a simplified seafloor treatment, the computations are relatively faithful to conditions during the experiment. Thirty-nine simulations were run in total. The only differences between the simulations were the *y* coordinates of the source positions. A sequence made from the results can imitate the effects of a wave packet moving past a fixed source, thus imitating the experiment.

The results show strong focusing and ducting, as expected. Sound intensity in vertical planes at *x* = 1500, 3000, 4500, and 6000 m from the edge containing the source is shown in Figure

978-1-4244-2126-8/08/$25.00 ©2008 IEEE

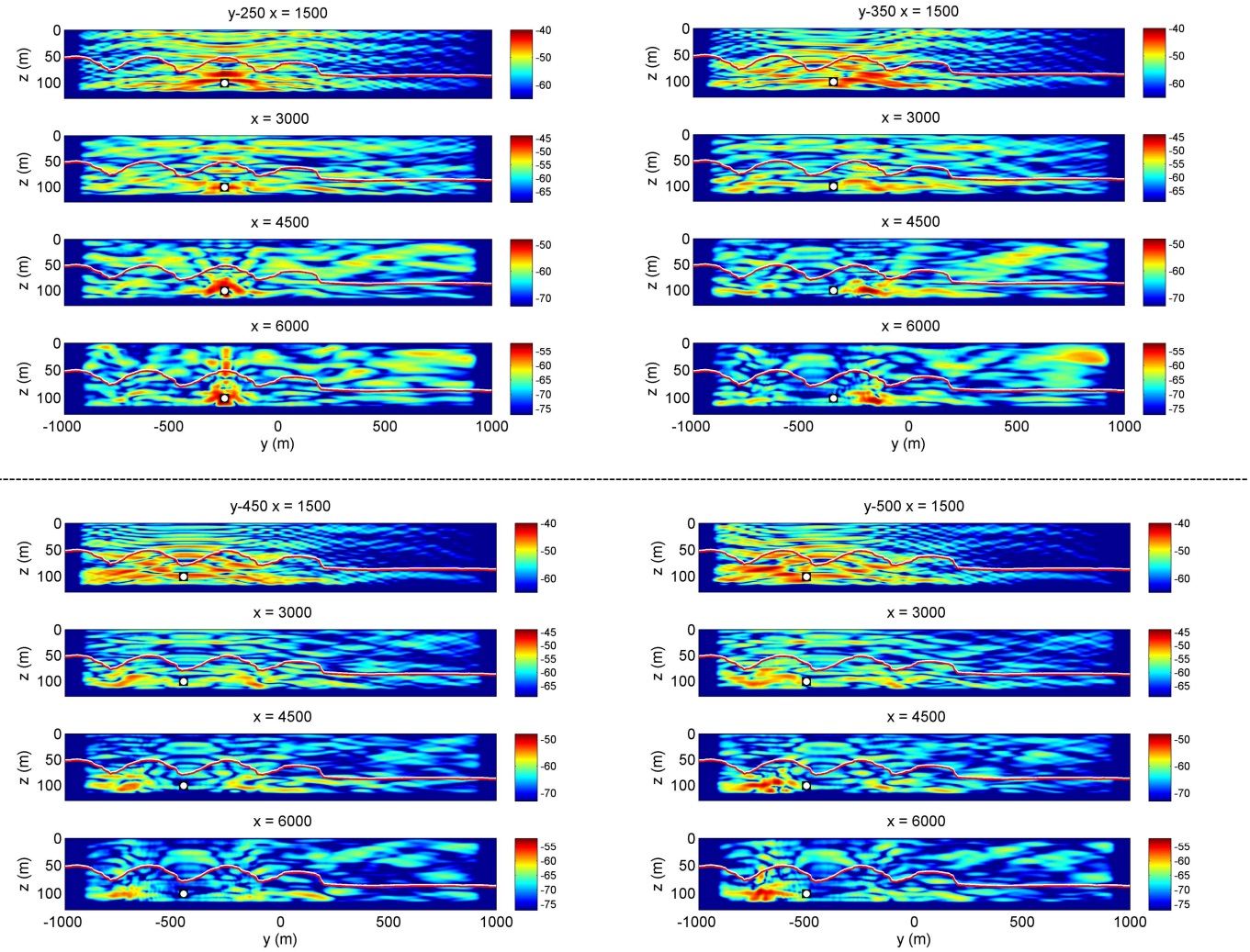

Fig. 8. Acoustic intensity in vertical planes from 3-D parabolic equation modeling is shown. The computation is as follows: An acoustic source is placed at x = 0 z = 101 m depth and four different y positions (shown with black and white symbols) in a Cartesian computational domain (upper left : y = -250 m, upper right : y = -350 m, lower left y = -450 m, and lower right y = -500 m. Intensity is shown in planes at 1500, 3000, 4500 and 6000 m (top to bottom in each quartet) , with 3000 and 6000 m corresponding to the distances from S1 to V1 and V2 in the experiment. The sound-speed field is derived from experimental temperature time series data taken at V1, converted to a spatial coordinates using observed wave speeds, and is x-independent. The 1530 m/s sound speed contour is shown, depicting four steep internal wave crests (which would move left to right) which serve as acoustic ducts. The upper-left case shows the source centered in a duct. See Figure 9 for plan views of the results.

8 for four runs. The view is through the plane towards the sound source, with the internal-wave propagation direction to the right. Also shown are the wave profiles in the form of 1530 m/s sound speed contours, and the source positions, which are fixed source depth z_s but have variable source position y_s for the four simulations shown. The simulation with y_s = -250 m has the source directly in a duct (internal wave crest), and the sound is seen to be channeled in the duct. When y_s = -350 m the source is to the left of the duct, as shown, and the sound is seen to also be trapped in the duct. At the 6 - km range the sound has not oscillated in the duct and has not returned to the source position y_s. For y_s the same behavior is seen, in mirror image. The simulations show the sound to be confined to a few hundred meters in y, about ½ the duct size, for these situations.

Plan views of the simulated depth-integrated intensity (similar to measured property E) are shown in Figure 9. The intensity is multiplied by distance from the source in order to reduce the dynamic range. This scaling eliminated the effects of cylindrical spreading which dominates after a few km, and allows a better view of ducting and seafloor-induced attenuation effects. The ducting can clearly be seen when the source lies in a duct, either centered in the duct or at the edge. Together, the two figures show the effects of the internal waves on the geometric shapes of high-intensity sound beams, and the level of intensity increase in the beams.

The thirty-nine runs completed at this time can provide a time-series view of the sound field of a fixed source at a fixed point, as observed in the experiment. Figure 10 shows a synthesized one-half hour long time series of results at range 6

978-1-4244-2126-8/08/$25.00 ©2008 IEEE

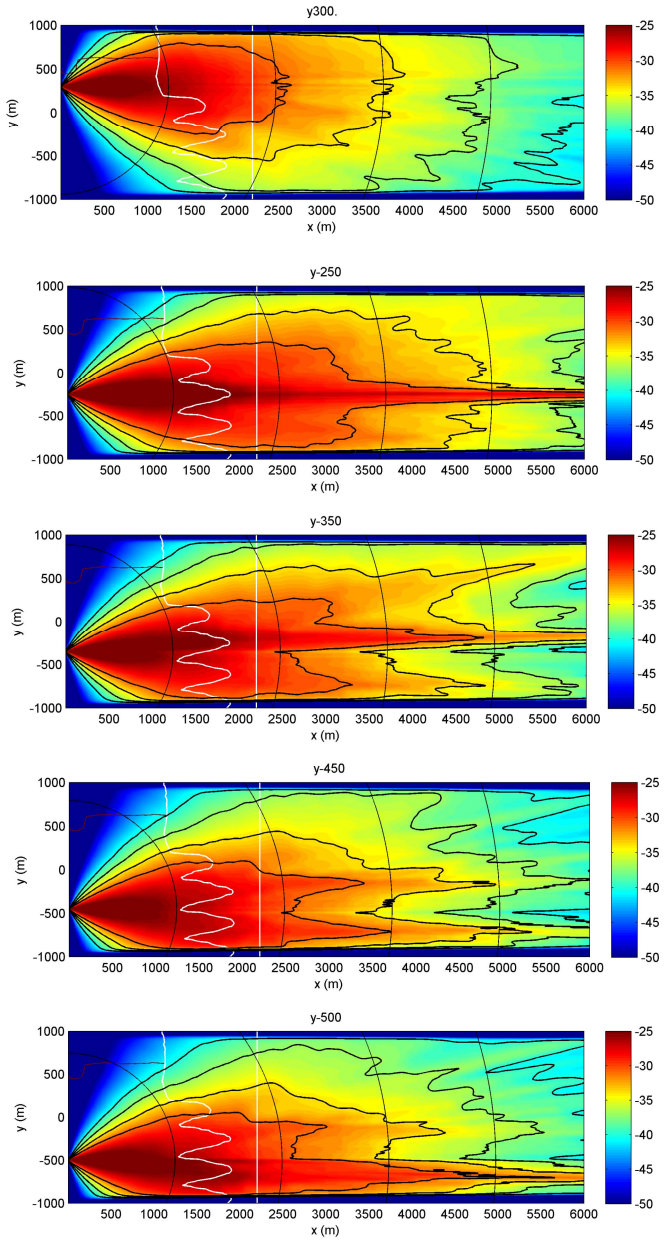

Fig. 9. Computational acoustics results. In plan view, depth-integrated intensity (similar to E), in relative dB, is shown, multiplied by distance from source to reduce spreading loss effects on the image. The contour interval is 3 dB. The profile of the internal wave field is shown in white, with the straight line showing the surface and the other line depicting 1530 m/s isovelocity depth (see Figure 7). The lower four panels show results from the simulations reported in Figure 8. The top panel shows results for a control case with the source in the long wave of depression that precedes the group of steep waves.

km at y position equal to y_s. The peaky structure of $E(t)$ seen at station V2 at the lower-right of Figure 6 is reproduced. (Note that a similar peaking of energy is seen for the situation of a moving receiver moving staying in a duct and a source moving past the duct, perpendicular to the internal wave crests, not shown). Further simulations and theoretical treatments, using more complex internal wave geometries, including curved waves and truncated ducts, can help quantify the range of fluctuations expected in complex sound-propagation environments such as observed in this experiment.

V. Summary

A short-distance fixed-path sound propagation experiment with auxiliary moored and ship-based environmental observations have provided detailed information about internal waves at a specific shelf location in the South China Sea, and about acoustic propagation through waves shapes found at a position a few km away from the shelf edge. At least nine packets of high-energy nonlinear internal waves moved over the acoustic path during the second half of the experiment. The strongest waves at the site come directly from a Luzon Strait wave source and interact strongly with shoaling topography before reaching the main experimental mooring site. These had crests aligned with the acoustic path, and typically had one very long and asymmetric wave of depression followed by an oscillatory wave train. The largest of the oscillatory waves had amplitudes near 30 m. Other nonlinear wave packets also passed by, some possibly generated locally via internal tide conversion, and others possibly being reflections of Luzon Strait waves from the Dongsha atoll (southwest of the moorings).

Sound convergence (ducting) and divergence is found to occur at short propagation ranges (3 and 6 km) for the very steep oscillatory internal waves. Intensity variance computed over 30-minute time windows is found to be highly variable and correlated with internal wave activity. Detailed analysis of events seen in time series of intensity measured with VLA receivers reveals evidence of horizontal sound ducting within the steepest and shortest of the internal waves. Initial

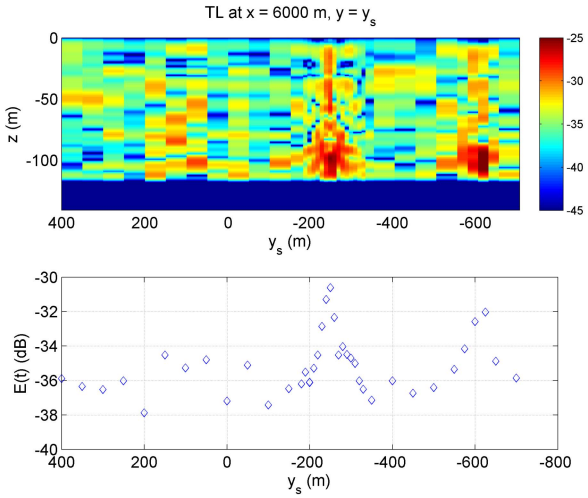

Fig. 10. Acoustic field properties from thirty 400-Hz 3D simulations are shown. For variable source position y_s the top panel shows transmission loss (intensity) in a duct at $y = y_s$ and $x = 6000$ m (see Figures 8 and 9). The lower panel shows depth-mean intensity *(*similar to *E)* at the same location. The horizontal axis is reversed so that a time series for a wave passing by a fixed-source/receiver geometry is imitated. For the observed wave speed, the figure shows approx ½ hour of time. More simulations are needed to have proper resolution throughout.

978-1-4244-2126-8/08/$25.00 ©2008 IEEE

computational modeling of sound propagating through structures similar to those observed has yielded results in qualitative agreement with observations. The three-dimensional parabolic equation method employed here may simplify modeling propagation through space- and time-varying environments because normal modes don't need to be computed throughout the domain to obtain results, and there are few restrictions such as adiabatic mode behavior.

ACKNOWLEDGMENT

Supporting grants from the Office of Naval Research are acknowledged. Use of the ship was funded by the Taiwan National Science Council. The scientific personnel on the cruise were Barry Ma (Chief Scientist, NA), Wen-Hua Her (NTU), Ming-Huei Chang (NTU), Shang Hong, Justin Chang, Ben Reeder (US–Chief Scientist, NPS), Chris Miller (NPS), Marla Stone (NPS), and Keith Wyckoff (NPS). The crew members and technicians of the NTU vessel *OR1* are thanked for their efforts.

REFERENCES

[1] Chang, M. -H., R.-C. Lien, T. Y. Tang, E. A. D'Asaro and Y. J. Yang, Energy flux of nonlinear internal waves in northern South China Sea, *Geophys. Res. Lett.,* vol. 33, L03607, doi:10.1029/2005GL025196, 2006.

[2] Ramp, S. R., T. Y. Tang, T. F. Duda, J. F. Lynch, A. K. Liu, Antony K; C.-S. Chiu, F. L. Bahr, H.-R. Kim, and Y.-J.Yang, Internal solitons in the northeastern south China Sea. Part I: sources and deep water propagation, *IEEE J. Ocean. Eng.,* vol. 29, pp. 1157-1181, 2004.

[3] Klymak, J. M., R. Pinkel, C.-T. Liu, A. K. Liu, and L. David, Prototypical solitons in the South China Sea, *Geophys. Res. Lett.,* vol. 33, doi:10.1029/2006GL025932, 2006.

[4] Lien, R.-C., T. Y. Tang, M. H. Chang, and E. A. D'Asaro, Energy of nonlinear internal waves in the South China Sea, *Geophys. Res. Lett.,* vol. 32, L05615, doi:10.1029/2004GL022012, 2005.

[5] Duda, T. F., J. F. Lynch, J. D. Irish, R. C. Beardsley, S. R. Ramp, C. -S. Chiu, T. W. Tang and Y. J. Yang, Internal tide and nonlinear internal wave behavior at the continental slope in the northern South China Sea, *IEEE J. Oceanic Eng.,* vol. 29, pp. 1105–1130, 2004.

[6] Yang, Y.-J., T. Y. Tang, M. H. Chang, A. K. Liu, M.-K. Hsu, and S. R. Ramp, Solitons northeast of Tung-Sha Island during the ASIAEX pilot studies, *IEEE J. Ocean. Eng.,* vol. 29, pp. 1182-1199, 2004.

[7] Orr, M. H., and P. C. Mignerey, Nonlinear internal waves in the South China Sea: Observation of the conversion of depression internal waves to elevation internal waves, *J. Geophys. Res.,* vol. 108, 3064, doi:10.1029 /2001JC001163, 2003.

[8] Headrick, R.H., J. F. Lynch, J. N. Kemp, A. E. Newhall, K. von der Heydt, J. R. Apel, M. Badiey, C.-S. Chiu, S. Finette, M. H. Orr, B. Pasewark, A. Turgut, S. N. Wolf and D. Tielbuerger, Acoustic normal mode statistics in the 1995 SWARM internal wave scattering experiment, *J. Acoust. Soc. Am.*, vol. 107, pp. 201-220, 2000.

[9] Chiu, C.-S., S. R. Ramp, C. W. Miller, J. F. Lynch, T. Y. Tang, Acoustic intensity fluctuations induced by South China Sea internal tides and solitons, *IEEE. J. Oceanic Eng*., vol. 29, pp. 1249-1263, 2004.

[10] Duda, T. F., J. F. Lynch, A. E. Newhall, L. Wu., and C.-S. Chiu, Fluctuation of 400-Hz sound intensity in the 2001 ASIAEX South China Sea Experiment, *IEEE. J. Oceanic Eng*., vol. 29, pp. 1264-1279, 2004.

[11] Mignerey, P. C., and M. H. Orr, Observations of matched-field autocorrelation time in the South China Sea, *IEEE. J. Oceanic Eng*., vol. 29, pp. 1280-1291, 2004.

[12] Badiey, M., B. G. Katsnelson, J. F. Lynch, S. Pereselkov, and W. L. Siegmann, Measurement and modeling of three-dimensional sound intensity variations due to shallow-water internal waves*, J. Acoust. Soc. Am.*, vol. 117, pp. 613-625, 2005.

[13] Miller, C. W., B. Reeder, M. Stone, and K. Wyckoff, Preliminary results from the Non-Linear Internal Wave Initiative (NLIWI) Acoustics Cruise, Technical Report, Naval Postgraduate School, Monterey, CA, 2007.

[14] Scotti, A., and J. Pineda, Observation of very large and steep internal waves of elevation near the Massachusetts coast, *Geophys. Res. Lett.,* vol. 31, L22307, doi:10.1029/2004GL021052, 2004.

[15] Vlasenko, V and K. Hutter, Numerical experiments on the breaking of solitary internal waves over a slope–shelf topography*, J. Phys. Oceanog.*, vol. 32, pp. 1779–1793, 2002.

[16] Preisig, J. C, and T. F. Duda, Coupled acoustic mode propagation through continental-shelf internal solitary waves, *IEEE. J. Oceanic Eng*., vol. 22, pp. 256-269, 1997.

[17] Duda, T. F., Initial results from a Cartesian three-dimensional parabolic equation acoustical propagation code, *WHOI Technical Report WHOI-2006-14*, Woods Hole Oceanographic Institution, Woods Hole, MA, 2006.

[18] Thomson, D. J., and N. R. Chapman, A wide-angle split-step algorithm for the parabolic equation, *J. Acoust. Soc. Am.,* vol. 74, pp. 1848-1854, 1983.

[19] Hardin, R. H., and F. D. Tappert, Applications of the split-step Fourier method to the numerical solution of nonlinear and variable coefficient wave equations, *SIAM Rev*., vol. 15, p. 423, 1973.